

Cascading Hazard Analysis of a Hospital Building

Original

Cascading Hazard Analysis of a Hospital Building / Marasco, Sebastiano; ZAMANI NOORI, Ali; Cimellaro, GIAN PAOLO.
- In: JOURNAL OF STRUCTURAL ENGINEERING. - ISSN 0733-9445. - ELETTRONICO. - 143:9(2017), p. 04017100.
[10.1061/(ASCE)ST.1943-541X.0001808]

Availability:

This version is available at: 11583/2674896 since: 2018-03-21T11:32:04Z

Publisher:

American Society of Civil Engineers (ASCE)

Published

DOI:10.1061/(ASCE)ST.1943-541X.0001808

Terms of use:

openAccess

This article is made available under terms and conditions as specified in the corresponding bibliographic description in the repository

Publisher copyright

(Article begins on next page)

CASCADING HAZARD ANALYSIS OF A HOSPITAL BUILDING

Sebastiano Marasco¹, Ali Zamani Noori², and Gian Paolo Cimellaro³

ABSTRACT

Recently, multi-hazards engineering has received more attention to analyzing the behavior of a system exposed to different types of hazards and to estimate the loss data from cascading events attributed to the primary hazard. In this paper, the principle of multi-hazards was investigated and a new methodology was developed to assess the total damage of structural elements caused by cascading hazards. For each hazard, a physical model is used to assess the conditional probability of exceeding a certain intensity level due to the occurrence of the previous hazard. The method was applied to a hospital located in California, US, subjected to the three cascading hazards (earthquake, blast, and fire). Non-linear time-history analyses were performed using seven ground motions scaled to five different earthquake levels and the seismic response of the structure was evaluated. The seismic input produces damage to the hospital's power supply (Liquid Propane Gas reservoir tank) which may cause a blast. The probability of explosion was estimated by taking into account the probabilities of fuel leakage, fuel concentration, and ignition. A set of nine blast intensity levels was considered in the analyses, corresponding to different quantities of fuel content inside the tank. Afterward, a fire hazard is generated following the explosion, whose intensity level was evaluated using the compartmental heat flux. The fire effects were modeled assuming an increment of temperature in the steel frames. The proposed multi-hazard approach can be used for both improving the structural safety and reducing the building life cycle costs to enhance in the end, the resilience of

¹Ph.D. Student, Department of Structural, Geotechnical and Building Engineering, Politecnico di Torino, Italy, E-mail: sebastiano.marasco@polito.it.

²Ph.D. Student, Department of Structural, Geotechnical and Building Engineering, Politecnico di Torino, Italy, E-mail: ali.zamani@polito.it.

³Visiting Professor, Department of Structural & Environmental Engineering, University of California, Berkeley, Berkeley, USA, E-mail: gianpaolo.cimellaro@polito.it.

the hospital. Results show that this methodology can be used to provide risk mitigation measures within a more general resilience framework.

Keywords: Cascading hazards; Earthquake; Fire; Blast; Damage; Resilience.

INTRODUCTION

Latest disasters have shown that large parts of the world are subjected to multiple natural, manmade, and artificial hazards. The rising of global population and the massive economic development in areas prone to disasters have increased the chance of multiple catastrophic incidents, which lead to disruption of buildings and infrastructures. After realizing that multi-hazard cannot be averted, modern societies are trying to enhance their capacity to withstand and to minimize the impact of multi-hazard on community infrastructure and human beings. Therefore, multi-hazard engineering and related mitigation risks are prompting attention in the topic of design and retrofitting of buildings and infrastructures.

The concept of multi-hazard is defined as the “implementation of methodologies and approaches aimed at assessing and mapping the potential occurrence of different types of natural hazards in a given area. The employed methods have to take into account the characteristics of the single hazardous events as well as their mutual interactions and interrelations” (Delmonaco et al. 2006). Multi-hazard design starts with the structural and non-structural analysis for individual hazard. The location, magnitude, and frequency of occurrence of each hazard have to be estimated through a probabilistic approach. Several probabilistic approaches have been proposed for multi-hazard risk assessment. A quantitative risk analysis of industrial facilities in a seismic area was carried out by Fabbrocino et al. (2005) taking properly into account the multi-hazard effects. An oil storage plant with several atmospheric steel tanks containing flammable materials was considered as a case study. The vulnerability of the steel tanks was estimated through a quantitative probabilistic seismic risk analysis. The response of the industrial equipment was expressed in terms of limit states defined in accordance with the post-earthquake damage observations and the consequence analysis was

48 performed. Asprone et al. (2010) assessed the blast damage for a four-story reinforced concrete
49 building in addition to seismic fragility. A possible blast scenario was assumed during the service life
50 of a building located in a seismic zone, and then the probability of progressive collapse was
51 calculated using a Monte Carlo simulation procedure.

52 Recent evaluation of post-disaster effects has led to the implementation of significant changes in the
53 modeling and numerical assessment of multi-hazards. Padgett et al. (2010) evaluated hazard
54 intensities to accurately predict the vulnerability of bridges using a multivariate regression analysis
55 of the data obtained by surveys after Hurricane Katrina.

56 More specifically, when considering multi-hazard, the assessment has to be performed by comparing
57 risks of cascading mechanisms related to the triggered hazard event. For instance, the impact of an
58 earthquake on a gas pipeline may initiate gas leakage, which may likely cause an explosion. There
59 are several examples of sequential hazards initiated by earthquakes which have caused fire such as
60 San Francisco (1906), Tokyo (1923), Kobe (1995), and Northridge (1994) earthquakes (Usmani
61 2008). The risk assessment of structures that are exposed to more than one hazard is determined by
62 adopting the performance-based approach. Bruneau et al. (2006) investigated the performance of
63 steel piers under seismic action. The simulation of large-magnitude earthquakes and the consequent
64 explosions confirmed the capacity of the materials to resist to earthquakes and blast separately, but
65 not a simultaneous combination of the two hazards (Bruneau et al. 2006). A novel assessment
66 method was suggested by Barbato et al. (2013) to evaluate the individual impacts of the interaction
67 among hurricane wind, flood, windborne debris, and rainfall hazards in the Performance-Based
68 Hurricane Engineering (PBHE) framework.

69 Furthermore, disasters are catastrophic to the socio-economic activities and affected communities
70 (Lindell et al. 2006). Federal Emergency Management Agency (FEMA) developed HAZUS-MH
71 (2011) to perform multi-hazard analysis. It is capable of estimating economic, physical and social
72 effects by providing access to the average annualized loss and probabilistic results from the hurricane
73 wind, flood and earthquake models and combining them.

74 The combination of cascading hazards to evaluate the real performance of a structure is among the
75 most difficult tasks due to the intricacy involved in the process. Although the use of current
76 probabilistic approaches is perceived as an important instrument to quantify the total loss, developing
77 a simplified probabilistic methodology is clearly challenging. In this paper, a new approach to
78 estimate the total amount of structural damage caused by series of cascading hazards is proposed.
79 Earthquake, blast, and fire were considered as sequential hazards and numerical analyses were
80 performed to assess the fragility functions for each hazard. The combination of the structural damage
81 for cascading hazards was evaluated according to Bayes' theorem. The conditional probability of
82 exceeding a certain intensity level due to the occurrence of triggered hazard with a given intensity
83 level was estimated by using physical models that take into account the vulnerability of a structural
84 component. The methodology was applied to a steel structure hospital located in California, US.
85 The first section of the paper will provide a detailed description of the proposed methodology, while
86 the second part will illustrate its applicability through a case study building. Lastly, a numerical
87 example of total structural damage estimation is performed.

88 **PROPOSED METHODOLOGY**

89 The application of the multi-hazard approach can improve the safety of structures and minimize life
90 cycle costs and human losses. In the Performance-Based Earthquake Engineering (PBEE) framework
91 (Porter 2003), the structural performance is conventionally expressed in terms of probability to
92 exceed a stated performance objective when the structure is subjected to a certain level of hazard as
93 follow:

$$94 \quad P(DV) = \iiint p(DV | DM) \cdot p(DM | EDP) \cdot p(EDP | IM) \cdot p(IM) \cdot dDM \cdot dEDP \cdot dIM \quad (1)$$

95 where DV identifies the Decision Variable, DM represents the Damage Measure, EDP is the
96 Engineering Demand Parameter, and IM is the Intensity Measure that characterizes the hazard.

97 The term $p(IM)$ represents the density probability function of exceeding a certain IM for a given
 98 hazard. In the case of cascading events, the correlation in terms of total exceedance probability of a
 99 given IM ($P(IM_i \geq im_i)$) has to be estimated through the associated conditional probability (see Fig. 1).
 100 $P(IM_i \geq im_i | IM_{i-1} \geq im_{i-1})$ represents the conditional probability of exceeding an IM for the i^{th} hazard
 101 ($IM_i \geq im_i$) due to a given IM for the $(i-1)^{th}$ hazard ($IM_{i-1} \geq im_{i-1}$).

102 In a multi-hazard scenario, the effects of different hazards combination (chain effects) have to be
 103 considered. The damage caused by the occurrence of a hazard generates a degradation of the
 104 Structural Parameters (SP) that influences the response of the structure subjected to the next
 105 sequential hazard. The PBEE framework for multiple cascading hazards is shown in Fig. 2. To
 106 consider the multi-hazard cascading effects, Eq. (1) can be rewritten as

$$107 \quad P(DV) = \iiint p(DV | DM) \cdot p(DM | EDP) \cdot p(EDP | IM, SP) \cdot \left[\prod_{i=2}^n p(IM_i | IM_{i-1}) \right] \cdot p(IM_1) \cdot p(SP) \cdot dDM \cdot dEDP \cdot dIM_1 \cdot dSP$$

108 (2)

109 where IM_1 indicates the intensity measure parameter associated with the main hazard (triggered
 110 hazard), the index i refers to i^{th} hazard, and n is the total numbers of cascading hazards.

111 Considering a multi-story building, the degradation of their structural characteristics (stiffness,
 112 strength, and damping) is evaluated according to FEMA P440A (FEMA 2009) (see Fig. 3).

113 Assuming a rigid horizontal diaphragm, the general component of the reduced stiffness matrix is
 114 calculated by

$$115 \quad k_{f,jj} = 12 \cdot \frac{E_{f,j} \cdot I_j}{h_j^3} \quad (3)$$

116 where $k_{f,jj}$ is the reduced stiffness component, $E_{f,j}$ is the reduced elastic modulus, and I_j and h_j are the
 117 inertia and height for the j^{th} story, respectively. The damping matrix is evaluated according to the
 118 Rayleigh formulation considering the reduced stiffness matrix.

119 The estimation of the probability of exceeding an IM for a hazard due to a given IM for the previous
 120 hazard is provided by using specific physical models. As an example, a steel tank containing
 121 flammable materials located in a seismic zone is considered. The probability to have an explosion of

122 the tank due to an earthquake with a given intensity level depends on the ignition mechanism of the
123 fuel content and on the failure modes of the tank. A physical model has to be capable of describing
124 the seismic fragility of the tank by identifying the most probable failure modes and the consequent
125 fuel release mechanism.

126 **CASE STUDY**

127 The case study considered earthquake, blast, and fire as series of cascading hazards. A five-story
128 steel building, located in Oakland, California, was designed according to the requirements of ASCE
129 7-10 (ASCE 2010). The basic building plan dimensions are 82.3 m (270 ft) by 33.7 m (110.5 ft),
130 with bays spanning of 9.1 m (30 ft) and 12.3 m (40.3 ft) in X and Y directions, respectively (see Fig.
131 4 and Fig. 5). The stories height is equal to 4.6 m (15 ft) and the structure was classified as regular in
132 both plan and elevation. The building is located on the relatively soft rock (site class C with
133 reference shear wave velocity ranging from 365.8 m/s (1200 ft/s) to 762 m/s (2500 ft/s) according to
134 ASCE 7-10 (ASCE 2010). The building has special steel moment resisting frame in the longest
135 direction (X-direction) and bracing system in the other direction (Y-direction). The designs of the
136 two considered lateral resisting systems are compliant with the code standards for design according
137 to the equivalent lateral force method (ASCE 2010). The W shape were used for beams and columns
138 while hollow structural sections (HSS) were designed for the bracing system (see Fig. 4 and Fig. 5).
139 The building's design comply with the occupancy category IV allowing the building to serve as a
140 hospital and accordingly an importance factor equals to 1.5 was considered in the seismic design.
141 The special steel moment resisting frame was designed with considering a response modification
142 factor (R) of 8 while the bracing system was designed with a response modification factor (R) of 6
143 considering the special steel concentrically braced frame according to ASCE 7-10 (ASCE 2010). The
144 P- Δ effects from the gravity columns were considered and the effects of large deformations of beam
145 and column elements were accounted for utilizing P- Δ nonlinear geometric transformation.

146 A standby power system was designed for providing an alternative source of electrical power for the
147 building and facilities in case of power outage. This system includes an above ground Liquid
148 Propane Gas (LPG) tank equipped with power sources, transfer equipment, controls, supervisory
149 equipment and accessory which are located outdoor. The tank was designed to provide a total power
150 of 2500 kVA and to maintain full capacity about 8 hours. The fuel capacity of the tank was assumed
151 equals to 718 l (190 gal) per hour at full load. Thus, the total LPG tank has a capacity of 3597 l (950
152 gal). The tank is 9.2 m (30 ft) away from the building according to National Fire Protection
153 Association (NFPA 2013). The Fig. 6 illustrates the geometric configuration of the LPG tank and
154 Fig. 7 shows its orientation with respect to the building.

155 The sequence of hazards triggered by the earthquake is not known and depends on the localization of
156 the high-risk potential elements inside and/or outside the analyzed structural system as well as their
157 level of damages. As an example, Fig. 8 represents the logical tree of multi-hazard sequence for
158 healthcare facilities.

159 The earthquake occurs and it causes damage to both building elements and external fuel tank. The
160 damaged tank may start fuel leakage and continues for a while in which gas ignites and causes
161 deflagration of the fuel inside the tank. Then, the explosion of the tank could generate an impulsive
162 air pressure load on the building façade which would cause localized damage to structural
163 components. The heat released by the tank explosion may cause the ignition of the inflammable
164 materials inside the buildings. In a short time, the ignition generates flashover and fire propagates
165 through the building compartment.

166 HAZARD ANALYSIS

167 Earthquake

168 The case study building is located in Oakland, California, US (Lat: 37.7792, Long: -122.1620).

169 Three hazard levels: 2%, 10%, and 50% probabilities of exceedance in 100 years were selected,
170 representing Collapse Prevention (CP), Life Safety (LS), and Immediate Occupancy (IO),

171 respectively (FEMA 2000). To better characterize the seismic hazard at the site, two additional sets
 172 of records representative of hazard levels at 5% and 20% probabilities of exceedance are also used in
 173 the analysis. The mean value of moment magnitude ($M_{W,mean}$) and epicenter distance (R_{mean}) with the
 174 logarithmic spectral offset at reference period ($\varepsilon(T_{ref})$) were evaluated according to Boore-Atkinson
 175 attenuation law (Boore and Atkinson 2008) for each Hazard Level (HL). All data can be found
 176 through the interactive de-aggregation of USGS (<http://geohazards.usgs.gov/deaggint/2008/>) (USGS
 177 2013). The shear wave velocity at the uppermost 30 m has been assumed equal to 736 m/s (2415 ft/s)
 178 according to Global Vs30 Map Server (<http://earthquake.usgs.gov/hazards/apps/vs30/>) (USGS 2013).
 179 A new Ground Motion Selection and Modification (GMSM) procedure (Marasco and Cimellaro
 180 2017) was used to minimize the dispersion values of the Engineering Demand Parameter (EDP)
 181 calculated through dynamic analyses. The new GMSM is based on the energy content in the
 182 frequency domain of the motions and it was carried out for the five HL. Seven groups of acceleration
 183 histories (for both horizontal directions) were selected for each HL in such a way to match the target
 184 spectrum at reference period of the building according to ATC P-58 (FEMA 2012). The Conditional
 185 Mean Spectrum (CMS- ε) obtained from the de-aggregation study was considered as target spectrum
 186 (Baker 2010). The Boore-Atkinson attenuation model (Boore and Atkinson 2008) was used to define
 187 the predicted spectral accelerations at the site (USGS 2013), while the Baker and Jayaram model was
 188 considered as correlation law (Baker and Jayaram 2010). Since the building is regular, the first
 189 period was selected as conditioning period (T_{ref}). The five CMS and the thirty-five groups of motions
 190 were obtained through the software OPENSIGNAL 4.1 (Cimellaro and Marasco 2015). A
 191 comparison between the target spectrum and the mean spectrum for HL of 2% and 5% in 100 years
 192 is depicted in Fig. 9 . For each HL, the mean spectrum was obtained as an average of the seven
 193 groups of spectra. The mean spectrum-compatibility is satisfied into the reference range of period
 194 (highlighted in grey in Fig. 9).
 195 Furthermore, the spectral acceleration at reference period ($S_a(T_{ref})$) was considered as seismic IM
 196 parameter in the analyses. Table 1 resumes the values of the IM parameters for each HL obtained

197 from the CMS-ε spectra. The maximum value of spectral acceleration denotes a strong seismic action
198 that may occur with a 2% of probability of exceedance in 100 years.

199 **Blast**

200 After an earthquake, the supply system (fuel tank, electrical components, etc.) may be slightly or
201 severely damaged. Damage in the valves, connections or pipes of a fuel tank generates a fuel leakage
202 that may cause an explosion. If the fuel concentration is less than the flammable concentration range
203 or if the ignition sources are lacking, the explosion cannot occur. The three main factors influencing
204 the explosion occurrence are the fuel leakage, concentration of fuel, and ignition source. Thus,
205 considering the three parameters as stochastic variables, the total conditional probability of
206 exceeding an IM for blast ($IM_B \geq im_B$) due to a given IM for earthquake ($IM_E \geq im_E$) is expressed as

$$207 \quad P(IM_B \geq im_B | IM_E \geq im_E) = P_L \cdot P_{FC} \cdot P_I \quad (4)$$

208 where P_L represents the probability of fuel leakage, P_{FC} is the probability to have maximum fuel
209 concentration and P_I defines the probability of ignition.

210 Since the tank is relatively small in size, it is reasonable to assume that the damage occurs in the pipe
211 connected to the tank. According to ATC P-58-2 (FEMA 2012), the probability to have large gas
212 leakage for small diameter piping system ($D < 2.5$ in) is given in terms of a fragility function with
213 accelerations as EDP ($\mu = 1.1g$, $\beta = 0.5$). The probability to have maximum gas concentration was
214 estimated considering the pipe failure relative to the rigid joint connection. A simplified dynamic
215 model was developed to assess the maximum horizontal drift of the pipe.

216 The tank was considered as a rigid body upon shear flexible legs. The tank is fully restrained at the
217 base by the anchor bolts designed according to ASCE 7-10 (ASCE 2010).

218 The dynamic behavior of the tank depends on the Fuel Quantity (F_Q) inside the tank. This parameter
219 was considered as a stochastic variable normally distributed and nine different exceedance
220 probabilities were considered as shown in Table 2. Since the LPG tank has to supply energy in the
221 emergency conditions, its fuel quantity during an earthquake may not be less than a given minimum

threshold. In the case study, a normal distribution of the fuel quantity was assumed with a mean value of 70% of the maximum quantity and standard deviation of 10. These parameters were selected to accomplish a reasonable functionality of the supplying tank in case of emergencies. Since the tank was designed to supply energy to the hospital in the case of power outage, the probability to have low fuel volume was assumed close to zero. Furthermore, the exceedance probability to have 100% of fuel quantity was fixed to 1.

Maximum fuel concentration (FC_{max}) is assumed to happen when the shear failure occurs in the vertical pipe. According to this hypothesis and considering the maximum shear stress value on the cross section of the pipe, the failure spectral acceleration ($S_{a,failure}$) is calculated by

$$S_{a,failure} = \frac{45.44}{g} \cdot \left(\frac{f_{u,d}}{E} \right) \cdot \left[\frac{L_v^3}{(D_e^2 - D_i^2)(D_e^2 + D_e \cdot D_i + D_i^2)} \right] \cdot \frac{1}{T_{tank}^2} \quad (5)$$

where $f_{u,d}$ and E represent the ultimate stress and elastic modulus of the steel, respectively, D_e and D_i are the external and internal pipe diameter, and L_v is the length of the vertical pipe, and g is the gravity acceleration.

The spectral acceleration at the reference period of the tank ($S_a(T_{tank})$) related to each selected ground motion was considered as the first IM parameter (IM_1) and fuel quantity as the second IM parameter (IM_2). Then, for each IM value, the spectral acceleration at the reference period of the tank was compared with failure spectral acceleration. When $S_a(T_{tank})$ is greater than $S_{a,failure}$, the failure of the pipe occurs and the probability to have maximum fuel concentration is assumed equal to 1 and 0 otherwise. Then, a tridimensional fragility surface was developed by fitting a lognormal distribution of the obtained results.

Ignition probability is estimated according to the maximum released fuel quantity. The charts provided by International Association of Oil and Gas Producers (IAOGP 2010) were used to estimate the probabilities of hydrocarbon releases ignition for several scenarios. The total ignition probability is considered as the sum of immediate and delayed ignition. Only delayed ignition probability was considered in the case study since immediate ignition needs sources close to the fuel leakage point.

247 The release of flammable gases from small onshore LPG plant was considered as ignition scenario
248 according to IAOGP (IAOGP 2010) and the related probability function was assumed (see Fig.
249 10(c)).

250 The probability of gas leakage, maximum gas concentration, and ignition are shown in Fig. 10.
251 Maximum gas concentration (FC_{max}) was calculated according to the Bernoulli's principle assuming
252 failure of the pipe ($FC_{max}=29.70 \text{ kg/s}$) and the related probability was derived (see Fig. 10(c)).
253 Finally, the conditional probability of exceeding an IM for blast ($IM_B \geq im_B$) due to a given IM for
254 earthquake ($IM_I = Sa(T_{tank}) \geq im_I$, $IM_2 = F_Q \geq im_2$) is calculated by using Eq. (2) (see Fig. 11).

255 The fuel quantity does not have a considerable influence while the spectral acceleration at the period
256 of the tank provides a sensitive contribution especially for values greater than 0.5 g.

257 **Fire**

258 The probability to have fire inside the building is related to the heat transmission due to the tank
259 blast. Assuming the nine different exceedance probabilities for the fuel quantity, the heat flux (q_f) for
260 each point of the building in front of the tank was calculated according to the Stefan Boltzmann's
261 law. The combustion temperature of LPG was assumed equal to 2300 K° (Costin 2014), the
262 transmissivity coefficient in the atmosphere as 0.66, and the transfer configuration factor was
263 calculated for the entire external panel of the building (meshed with 0.5×0.5 m elements). Only the
264 opening surfaces (windows, doors, etc.) on the façade were considered as susceptible to trigger fire
265 inside the building. The internal walls are located between each two adjacent columns. Furthermore,
266 the ceiling and the internal walls of the building are composed by fireproof gypsum plasterboard
267 with steel studs. Thus, each fire compartment was identified as the volume confined between
268 adjacent columns (see Fig. 12) and ceiling.

269 The minimum value of heat flux capable of igniting the common flammable materials in a room was
270 assumed equal to 30 MJ/m² (Babrauskas and Krasny 1985). For each considered fuel quantity, the
271 surfaces of the building façade having a heat flux greater than 30 MJ/m² is identified (see Fig. 13).

272 The fire may propagate through the opening surfaces located within the heat flux surface for a given
273 fuel quantity (see Fig. 13) and the number and localization of the compartments under fire were
274 identified (see Table 3).

275 When the calculated heat flux is greater than the considered limit, the estimated conditional
276 probability to have ignition of elements inside the building was assumed equal to 1, and 0 otherwise.
277 The conditional probability of exceeding an IM for fire ($IM_F \geq im_F$) due to a given IM for blast
278 ($IM_B = F_Q \geq im_B$) was estimated ($P(IM_F \geq im_F / IM_B \geq im_B)$) by fitting a lognormal distribution of the
279 obtained results (see Fig. 14). A mean $\mu=40\%$ and standard deviation $\beta=0.95$ were estimated for the
280 lognormal cumulative density probability (see Fig. 14).

281 282 **STRUCTURAL ANALYSIS**

283 **Earthquake**

284 The time history analyses were performed on a three-dimensional steel structure utilizing SAP2000
285 (Computers and Structures, Inc.). The nonlinearity of the structural elements was taken into account
286 according to concentrated plasticity model. According to FEMA 356 (FEMA 2000), *Steel-beams*
287 *Flexural Hinge* (type *Moment M3*) was used for beam elements while *Steel-column Flexural Hinge*
288 (type *P-M2-M3* with $M-\chi$ cylindrical domain) was applied for columns. The plastic hinges for brace
289 elements were modeled as *Steel-braces Axial Hinges*. 3% of damping ratio was assigned to the
290 frames using Rayleigh damping formulation with control frequency of 1.00 and 2.85 rad/s. The
291 nonlinear dynamic analyses were performed using non-linear direct integration method, taking into
292 account P- Δ effects and applying the horizontal acceleration time histories in the two principal plan
293 directions of the building model.

294 **Blast**

295 Estimation of blast load parameters was focused in the number of studies during the last decades and
296 several methods were proposed to determine the explosion wave properties. U.S. Army Technical
297 Manual (TM5-1300 1990) is a widely used standard which presents a series of charts to determine

the basic parameters of blast loads. Charts provided by TM5-1300 were used in order to establish the blast load parameters required in structural analysis. As a general practice, the magnitude and distribution of the blast load are a function of the quantity of output energy released by detonation, charge weight (W), and the stand-off distance of explosive relative to the particular target (R). W is expressed as an equivalent weight of trinitrotoluene (TNT) and blast wave demands were determined in a function of universal scaled distance parameter ($Z = R / W^{1/3}$). TNT equivalent charge weight of LPG fuel is given by (Sutton et al. 1975)

$$W_{TNT} = \varepsilon \frac{\Delta H_{C_{LPG}} W_{LPG}}{\Delta H_{C_{TNT}}} \quad (6)$$

where W_{TNT} is TNT equivalent charge weight of LPG (kg), W_{LPG} is weight of LPG (kg), and $\Delta H_{C_{LPG}}$ is LPG heat of combustion equals to 1.099×10^7 (cal/kg), $\Delta H_{C_{TNT}}$ is TNT heat of combustion equals to 1.109×10^6 (cal/kg). The unitless parameter ε is a term empirically equals to 0.1, and takes in account the partial combustion and physical difference between TNT and gaseous explosion. In addition, an empirical weight equivalency factor to consider the effect of the tank shell was considered as (SBEDS 2008).

$$W_b = \left[0.2 + \frac{0.8}{(1 + W_c / W)} \right] W \quad (7)$$

where W_b is equivalent bare charge weight (kg), W is charge weight inside casing (kg), and W_c represents the weight of casing (kg). The spectral accelerations of the tank for each HL were considered as first IM (IM_1), while nine different fuel quantities representative of the second IM (IM_2) (ranging from 55% to 100%) were assumed for performing blast analyses were considered (see Table 2).

Detonation of an explosive releases a large-scale of energy in terms of compressed air in a short period of time (blast wave). Blast wave generates an instantaneous rise to the value of pressure (P_{so}) above ambient pressure (P_o). Then blast shock expands with very high velocity outward from the

explosion source into the surrounding areas (positive-pressure phase). As the blast wave travels into increasingly larger areas, the energy of blast wave is dissipated and positive incident pressure at the front decays. Within milliseconds of time, the air front pressure may drop below the normal atmospheric pressure over the time period (t_o) which creates partial vacuums (negative-pressure phase). The negative phase is usually of a longer duration (t_o^-) than the positive phase and its amplitude (P_{so}^-) is less than the ambient atmosphere pressure. When the blast wave encounters structure, reflection increases the overpressure to a maximum pressure (P_r) which is greater than the peak incident pressure (P_{so}) (see Fig. 15(a)).

The reflected pressure is a function of the incident angle (between the shock wave and the line perpendicular to the target surface) and the incident pressure. The maximum reflected pressure and corresponding total reflected impulse (i_r) were calculated through provided charts by TM5-1300. For design purpose, the blast time history overpressure was idealized by rising of an equivalent triangular pulse of maximum reflected pressure at an arrival time (t_A) after the explosion (see Fig. 15(b)). The actual positive duration was replaced by a fictitious duration (t_{rf}) assuming the linear decay of overpressure is given by (TM5-1300 1990)

$$t_{rf} = 2i_r / P_r \quad (8)$$

A similar procedure for determining the negative fictitious duration (t_{rf}^-) was used whereas rising time of negative peak pressure is considered equal to $0.25 \cdot t_{rf}^-$. Different blast pressure time histories specific to each member were established corresponding to the different scaled distance parameter (Z) and potential charge weight for each blast IM.

The blast load was applied to beams, columns and exterior walls on the exposed structural area on the front face of the explosion. The reflection areas of the building were assumed big enough in order that there is no blast wave diffraction around the structure. Exterior walls were considered as typical concrete masonry wall reinforced with vertical bars. Since the vertical span of the wall is less than the horizontal span, and also the connection between the wall and adjacent columns are typically weak, the most of the wall strength and stiffness is provided by the vertical direction. Hence the wall

347 components were considered as one-way spanning elements that can transfer only the equivalent
348 static reaction load to the adjacent beams.

349 To do blast analysis, each wall was simplified as a Single Degree Of Freedom (SDOF) system. The
350 mass, stiffness and actual force of the wall were transformed into an equivalent system so that the
351 deflection of the concentrated mass is the same as the mid-span of the actual wall (Biggs 1964). An
352 elasto-perfectly plastic behavior for the wall was considered taking into account its dynamic
353 characteristics under the high-velocity impacts (TM5-1300). The dynamic responses of the mid-span
354 of the wall, considering the plastic hinge development (yield rotation capacity), were determined.
355 Resulted time history reactions were calculated and directly applied to the adjacent beams in
356 SAP2000 models (Computers and Structures Inc.) considering the rigid diaphragm for each floor.
357 For the columns and beams, blast pressure time histories were determined and the corresponding
358 pressures-time functions were applied directly on framing elements. The structural stiffness
359 reduction caused by the earthquake was assessed according to FEMA P440A (FEMA 2009)
360 degradation model. For each seismic IM, the mean values of stiffness reduction for the selected
361 seven groups of ground motions were considered.

362 Mechanical properties of steel materials were enhanced by means of Dynamic Increased Factors
363 (DIF) in order to take into account the effects of high rapid load environment compared to static
364 loading conditions (TM5-1300 1990). Since the blast load duration is very short compared to the
365 fundamental natural period of the structure, the structural damping effects were not considered in the
366 analyses. Transmission of the ground shock induced by the explosion to the foundation of the
367 structure was not considered in this study. Finally, nonlinear time history analyses were carried. In
368 the cases of the loss of the load-bearing capacity of key structural components, the progressive
369 collapse analyses were performed and the dynamic effects of removal of the failed elements were
370 evaluated using time history analyses.

371 **Fire**

372 After ignition of inflammable materials inside the compartment, flashover occurs causing an increase
 373 in temperature. Design-basis fire standards are based on the evaluation of post-flashover time-
 374 temperature relationships (fire curve) for the compartment. Naturally, the fire curve depends on the
 375 quantity of combustible materials (total calorific value), the velocity of combustion, and the
 376 ventilation conditions. The first two parameters affect the total heat flux generated within the
 377 compartment (q_f). According to Euro Code 1 (EC1, 2002), the specific fire load is given in terms of
 378 mean value and standard deviation of a normally distributed function for different building
 379 categories. For hospitals, the mean specific fire load of 230 MJ/m² and the standard deviation of 69
 380 are suggested. In the study case, the specific heat flux of the compartment was selected as first IM
 381 (IM₁) and eight different exceedance probabilities were considered as shown in Table 4.

382 The fuel quantity inside the tank was assumed as second IM parameter (IM₂).

383 Since temperature-time relationships are not suitable to describe the real post-flashover behavior
 384 (growth phase, steady-burning phase, and decay phase), several idealized temperature-time functions
 385 were developed. In this study, the temperature-time relationship developed by Lie (Lie et al. 1974)
 386 was considered as given below

$$387 \quad \begin{cases} T = 250 \cdot (10 \cdot F)^{0.1/F^{0.3}} \cdot \exp(-F^2 \cdot t) \cdot [3 \cdot (1 - \exp(-0.6 \cdot t)) + \\ - (1 - \exp(-3 \cdot t)) + 4 \cdot (1 - \exp(-12 \cdot t))] + C \cdot \left(\frac{600}{F}\right)^{0.5} \\ T = -600 \cdot \left(\frac{t}{t_{peak}}\right) - 1 + T_{peak} \end{cases} \quad (9)$$

388 The first expression describes the heating phase, while the second one is referred to the cooling
 389 phase. The ventilation conditions are considered by means of the opening factor F
 390 ($F = A_v \cdot (H)^{0.5} / A_c$), where A_v is the total surface of vertical openings, H is the height of openings,
 391 and A_c is the area of the compartment. Two vertical openings with 1.50 m×2.00 m were assumed for
 392 each compartment (see Fig. 12) and the opening factor of 0.07 was calculated.

393 The constant C is associated with the type of burned materials and it is assumed equal to 1 for light
 394 materials and 0 for heavy ones. The top of the curve is described by peak time (t_{peak}) and peak
 395 temperature (T_{peak}). These two parameters define the fire severity inside the compartment. These
 396 parameters were defined according to the time equivalence concept, that relates the real fire exposure
 397 to the standard test fire (standard curve). EC1 (EC1 2002) proposes the calculation of the equivalent
 398 time t_e expressed as

$$399 \quad t_e = k_b \cdot w \cdot q_f \quad (10)$$

400 where q_f is the fire load in terms of heat flux and k_b is a parameter taking into account the different
 401 compartment lining (generally equal to 0.07 min m²/MJ). Considering only vertical openings in
 402 compartment, the ventilation factor w is given by

$$403 \quad w = \left(\frac{6}{H_c} \right)^{0.3} \cdot \left[0.62 + 90 \cdot \left(0.4 - \frac{A_v}{A_c} \right)^4 \right] \quad (11)$$

404 where H_c defines the height of the compartment.

405

406

407

408

409

410

411

412 **Table 5** resumes the main parameters of the temperature-time curves for each generated heat flux.

413 According to the obtained results listed in

414

415

416

417

418

419

420 **Table 5**, the slope of the heating curve (T_{peak}/t_{peak}) decreases with the increasing of the generated heat
 421 flux into the compartment.

422 Degradation of the physical and mechanical characteristics of the materials and the actions due to the
 423 fire were evaluated. According to Fourier's equation, the thermal distribution depends on the net
 424 transmitted heat flux ($q_{f,n}$) in the time for a given fire scenario. Assuming all the structural elements
 425 as homogeneous and isotropic, the Fourier's problem can be integrated into the volume of the
 426 element and rewritten in the discrete form as (EC3 2005)

$$427 \quad \Delta T_{(i)} = k_{sh} \cdot \frac{A_m / V}{\rho \cdot c} \cdot q_{f,n(i)} \cdot \Delta t \quad (12)$$

428 where $\Delta T_{(i)}$ defines the i^{th} increment of uniform temperature in the element cross section and A_m/V is
 429 the section factor given by the ratio between the area of the element exposed to fire (A_m) and its total
 430 volume (V). Density (ρ) and specific heat (c) are referred to the material composing structural
 431 element while Δt is the time step in which the increase of temperature occurs ($\Delta t < 5s$). The fire
 432 protection system effect was neglected in the fire analysis. The current fire codes do not address the
 433 compound effects of hazards in a sequential manner. In fact, the damage to structural elements due to
 434 earthquake and blast, causes partial loss of fire protection (e.g. cracking of fireproof cladding,
 435 peeling of fireproof painting, etc.). Since in this case study, the fire load was applied on the structure
 436 damaged by sequential earthquake and blast, all the measures for fireproofing are deteriorated. The
 437 estimation of fire protection loss percentage is out of this study, then the total loss of fireproof
 438 system was considered as the worst case.

439 The coefficient k_{sh} takes into account the "shadow effects" that is responsible for a non-uniform
 440 thermal transversal distribution. In order to consider a pseudo-uniform transversal temperature
 441 distribution, the k_{sh} coefficient was considered according to the real fire exposure. Parameter $k_{sh}=0.7$
 442 was assumed for beams (fire exposure on three sides) and $k_{sh}=0.9 \cdot (A_m / V)_b / (A_m / V)$ was

443 considered for columns according to Eurocode 3 (EC3 2005). The ratio $(A_m/V)_b$ is the section factor
444 of the element that was assumed as bin section and (A_m/V) is the real section factor of the column.
445 The fire exposure for the column was supposed for one side of the web and for both flanges. Three
446 different section of beams and columns have been identified for the compartment. Table 6
447 summarizes the uniform temperature on the steel cross sections of the compartment at t_{peak} time for
448 each heat flux value where the sections W12x136 and W14x109 identify the columns and the section
449 W21x44 is related to the beams inside the compartments.

450 Fire resistance of steel elements inside the compartment was evaluated considering the maximum
451 uniform thermal loads for each heat flux value. The software SAP2000 (Computers and Structures
452 Inc.) was used to perform the analyses. The mechanical and physical materials properties were
453 modified according to AISC (AISC 2005) depending on the temperature value. The nonlinearity of
454 the structural elements was taken into account according to concentrated plasticity model and the
455 progressive nonlinear analyses were performed. The structural stiffness reduction caused by the
456 earthquake and blast was assessed according to FEMA P440A (FEMA 2009) degradation model. For
457 each seismic IM the mean values of stiffness reduction for the selected seven groups of ground
458 motions were considered. The reduced stiffness, strength, and damping were also calculated for each
459 selected fuel quantity value.

460 **DAMAGE ANALYSIS**

461 **Earthquake**

462 A common approach is to correlate the performance of structural elements to one or more EDPs
463 based on peak inter-story drifts. Peak inter-story drifts are capable of providing information about
464 the damage state of the elements. According to ATC P-58 (FEMA 2012), four Earthquake Damage
465 States (DS_E) (slight, moderate, extensive, and complete) have been identified for the steel building
466 depending on the transient drift ratio. The associated fragility curves are provided for both horizontal
467 directions using the four DS_E (see Fig. 16).

468 **Blast**

469 In blast analyses, the evaluation of the structural building performance based on inter-story drifts
470 limits the investigation to maximum local damage. The blast causes a damaged localized on the
471 structural components depending on the distance to the blast source. In the case of intense blast load,
472 a partial collapse may occur causing a redistribution of the actions in the slightly damaged
473 components. Thus, the estimation of the damage on a building has to take into account the global
474 behavior of the structure. In order to accurately assess the global response of a building under blast
475 load, the loss of horizontal stiffness was assumed as EDP. The evaluation of the structural global
476 response requires the maximum lateral displacements shape of the building due to the blast and the
477 total induced elastic action. In the case study, the response of the structure in Y direction (see Fig. 5)
478 was assimilated to a SDOF dynamic response given by

$$479 \quad K_{eq} = \frac{\delta_{eq}}{V_{eq}} = \frac{\delta_{top} \cdot \sum_{i=1}^{N=5} (\phi_i - \phi_{i-1})^2}{V_b \cdot \sum_{i=1}^{N=5} \phi_i} \quad (13)$$

480 where δ_{top} is the maximum top floor displacement and V_b is the base shear resulted at the same time
481 of the maximum displacement. The real distribution of floor displacements was taken into account
482 through the shape coefficients ϕ_i that represents the i^{th} floor displacement normalized with respect
483 the top one. Table 7 resumes the horizontal stiffness reduction for each selected fuel quantity level
484 derived from the performed progressive collapse analyses. The lateral stiffness reduction was
485 calculated for each selected earthquake scenario considering the chain effects. Thus, the degradation
486 of the structural parameters was evaluated and the blast load was applied on the structure with
487 modified mechanical characteristics. The first column of Table 7 represents the five different HLs for
488 earthquake while the first row identifies the nine HLs selected for the fuel quantity.

489 The yield drift for the braced system was calculated according to ATC P-58 (FEMA 2012) and the
490 maximum drift threshold was assumed for four different damage states. The stiffness reduction limits
491 were calculated assuming an elasto-perfectly plastic global behavior of the steel frame (see Table 7).

492 According to the estimated stiffness reduction values for each damage state, the associated
493 exceedance probability ($P(DS_B \geq ds_B)$) surfaces were evaluated (see Fig. 17).

494 **Fire**

495 The structural capacity assessment was carried out considering maximum deflection for beams and
496 columns as EDP. Two different damage states were assumed:

- 497 - Fire Damage State 1 ($DS_{F,1}$): irreversible damage on the beam with maximum response;
- 498 - Fire Damage State 2 ($DS_{F,2}$): irreversible damage in the column with maximum response.

499 The first damage state gives information about the maximum flexural capacity of the beam. The
500 threshold vertical deflection (v_b) for this damage state was assumed equal to the deflection causing
501 an uncontrolled vertical displacement (Gernay et al. 2016). The second damage state is related to the
502 maximum drift of the column (δ_c) under multiple stresses due to compression and bending moment,
503 taking into account the P- Δ effects. The maximum limit for the drift was assumed coincident with the
504 horizontal displacement that produces uncontrolled unstable displacement (Gernay et al. 2016).

505 Several analyses were performed considering the different fuel quantity and heat ratio as HLs. The
506 degradation of the structural parameters was evaluated and the fire load was applied on the structure.
507 For each analysis, the probability to have irreversible damage to the structural elements was assumed
508 equal to 1 if the response parameter is greater than the associated limit and 0 otherwise.

509 The probability of exceeding certain damage state due to the fire hazard ($P(DS_F \geq ds_F)$) was developed
510 fitting lognormal distribution to the obtained data (see Fig. 18).

511 **NUMERICAL EXAMPLE**

512 The total probability of exceeding a given damage state was derived according to Eq.(2). In a
513 cascading multi-hazard scenario, the probability of exceeding a given damage state has to be
514 calculated considering the conditional probability of exceeding a certain intensity level due to the
515 occurrence of the previous hazard. For the case study, earthquake-blast-fire was considered as
516 cascading hazards. According to the numerical analyses performed and considering a complete

517 damage to the columns of the building as damage state, the probabilities of exceeding the selected
518 level of damage was estimated for the three hazards.

519 The spectral acceleration at the period of the structure, fuel quantity inside the tank, spectral
520 acceleration at the period of the tank, and heat flux generated in the compartment were assumed as
521 IM parameters. A numerical example was carried out with reference to the five different HL for the
522 earthquake, 80% of the full capacity of the tank and heat flux equal to the average value. Table 9
523 shows exceedance damage probability values for the case study building and the conditional
524 probability of exceeding an IM for the one hazard due to a given IM for the previous hazard. The
525 complete damage on the columns was selected as damage state and then the associated exceedance
526 damage probability ($P(DS > ds)$) was estimated.

527 It is clear that the probability to have blast after the earthquake is correlated to the size of the tank. In
528 the case study, a low conditional probability of exceeding an IM for the blast due to a given IM for
529 the earthquake was associated with the value of maximum gas concentration. But, for the cases of
530 farm tanks, the conditional probability value may be considerable.

531 **CONCLUDING REMARKS**

532 Recent experiences have shown that buildings and infrastructures are significantly vulnerable to
533 multi-hazard effects. The combination of cascading hazards is essential to evaluate the real
534 performance of a structure and the respective economic losses. This study presented a new approach
535 to assessing the conditional probability of exceeding a certain intensity level due to the occurrence of
536 the previous hazard, estimating the exceedance damage probability and taking into account the
537 interdependency between different hazards. The main novelty of this research is the estimation of
538 exceedance damage probability for a given damage state due to earthquake, blast and fire hazard by
539 considering the physical models. The method can be considered as an alternative to the Monte Carlo
540 simulations, thus it reduces the computational time to perform the analyses, but it requires accurate
541 calibration of the physical parameters which plays a key role in reducing the epistemic uncertainty of

the model. In addition, the degradation of the structural parameters was taken into account for correctly assessing the performance of a structure subjected to cascading hazards. The application of the proposed cascading multi-hazard approach can be used for both improving the structural safety and reducing the building life cycle costs to enhance the resilience of the structure.

ACKNOWLEDGEMENTS

The research leading to these results has received funding from the European Research Council under the Grant Agreement n° ERC_IDEAL RESCUE_637842 of the project IDEAL RESCUE—Integrated Design and Control of Sustainable Communities during Emergencies.

References

- AISC (2005). "Specification for Structural Steel Buildings." AISC 360, American Institute of Steel Construction, Chicago, IL.
- ASCE. (2010). "Minimum design loads for buildings and other structures." 7-10, Reston, VA.
- Asprone D., Jalayer F., Prota A., and Manfredi G. (2010). "Proposal of a probabilistic model for multi-hazard risk assessment of structures in seismic zones subjected to blast for the limit state of collapse." *Structural Safety*, Volume 32, Issue 1, Pages 25-34.
- ATC (2012). "Seismic Performance Assessment of Buildings." ATC-58, *Applied Technology Council*, Redwood City, CA.
- Babrauskas V., and Krasny J.F. (1985). "Fire Behaviour of Upholstered Furniture." *NBS Monograph 173* (U.S.), National Bureau of Standards.
- Baker, J. W. (2010). "Conditional mean spectrum: Tool for ground-motion selection." *Journal of Structural Engineering*, 137(3), 322-331.

567 Baker, J. W., and Jayaram, N. (2008). "Correlation of spectral acceleration values from NGA ground
568 motion models." *Earthquake Spectra*, 24(1), 299-317.

569 Barbato, M., Petrini, F., Unnikrishnan, V. U., and Ciampoli, M. (2013). "Performance-Based
570 Hurricane Engineering (PBHE) framework." *Structural Safety*, 45, 24-35.

571 Biggs, J. M. (1964). *Introduction to structural dynamics*, McGraw-Hill, New York.

572 Boore, D. M., and Atkinson, G. M. (2008). "Ground-motion prediction equations for the average
573 horizontal component of PGA, PGV, and 5%-damped PSA at spectral periods between 0.01 s
574 and 10.0 s." *Earthquake Spectra*, 24(1), 99-138.

575 Bruneau, M., Lopez-Garcia, D., and Fujikura, S. "Multihazard-resistant highway bridge bent." *Proc.*,
576 *Proc., Structures Congress*, ASCE New York, 1-4.

577 Cimellaro, G. P., and Marasco, S. (2015). "A computer-based environment for processing and
578 selection of seismic ground motion records: Opensignal." *Frontiers in Built Environment*, 1,
579 17.

580 Computer and Infrastructure Inc. SAP2000, Version 17.3, Berkeley, CA.

581 Costin, N. S. (2014). "Numerical simulation of detonation of an explosive atmosphere of liquefied
582 petroleum gas in a confined space." *Defence Technology*, 10(3), 294-297.

583 Delmonaco, G., Margottini C., and Spizzichino D. (2006). "Report on new methodology for multi-
584 risk assessment and the harmonisation of different natural risk maps." *Deliverable 3.1*,
585 *ARMONIA*.

586 EC (2002). "Eurocode 1: Actions on structures." *Part 1-1: General actions - Densities, self-weight*,
587 *imposed loads for buildings*, EC1, European Committee for Standardization, Bruxelles, BG.

588 EC (2005). "Design of steel structures - Part 1-2: General rules -Structural fire design." *EC3*,
589 *European Committee for Standardization*, Bruxelles, BG.

590 Fabbrocino G., Iervolino I., Orlando F., and Salzano E. (2005). "Quantitative risk analysis of oil
591 storage facilities in seismic areas." *Journal of Hazardous Materials*, Volume 123, Issues 1–3,
592 Pages 61-69.

593 FEMA (2000). "Prestandard and Commentary for the Seismic Rehabilitation of Buildings." FEMA
594 356, Federal Emergency Management Agency, Washington, D.C.

595 FEMA (2009). "Effects of Strength and Stiffness Degradation on Seismic Response." FEMA P440A,
596 Federal Emergency Management Agency, Washington, D.C.

597 FEMA (2011). "Hazus FEMA's methodology for estimating potential losses from disasters ", FEMA
598 Federal Emergency Management Agency, Washington, D.C.

599 Gernay, T., Khorasani, N. E., and Garlock, M. (2016). "Fire fragility curves for steel buildings in a
600 community context: a methodology." *Engineering Structures*, 113, 259-276.

601 IAOGP (2010). "Ignition probabilities." *Risk Assessment Data Directory*, International Association
602 of Oil & Gas Producers, Report No. 434-6.1.

603 Lie, T. T. (1974). "Characteristic temperature curves for various fire severities." *Fire Technology*,
604 4pp. 315-326.

605 Lindell, M. K., Perry, R. W., Prater, C., and Nicholson, W. C. (2006). "Fundamentals of emergency
606 management". Washington, DC: FEMA. Chicago.

607 Marasco, S., Cimellaro, G.P. (2017). "A new energetic based ground motion selection and
608 modification algorithm.". *Proc., 16th World Conference on Earthquake Engineering*,
609 Santiago, Chile.

610 NFPA 30 (2013). "Flammable and Combustible Liquids Code." Committee on Tank Storage and
611 Piping Systems.

612 Padgett, J., Ghosh, J., and Ataei, N. (2010). "Sensitivity of dynamic response of bridges under
613 multiple hazards to aging parameters." *Proc., 19th analysis and computation specialty
614 conference. ASCE*.

615 Porter, K.A. (2003). "An overview of PEER's performance-based earthquake engineering
616 methodology." *Proc. Ninth International Conference on Applications of Statistics and
617 Probability in Civil Engineering (ICASP9)* July 6-9, 2003, San Francisco, CA. Civil

618 Engineering Risk and Reliability Association (CERRA), 973-980.
619 <http://www.sparisk.com/pubs/Porter-2003-PBEE-Overview.pdf>.
620 SBEDS (2008). "Methodology Manual for the Single-Degree-of Freedom Blast Effects Design
621 Spreadsheets." *PDC TR-06-01 Rev 1*, Protective Design Center Technical Report, U.S. Army
622 Corps of Engineers.
623 Sutton, S. B., and McCauley, E. W. (1975). "Assessment of Hazards Resulting from Atmospheric
624 Propane Explosions at LLL.", US Energy Research and Development Administration,
625 California Univ., Livermore Lawrence Livermore Lab.
626 TM5-1300 (1990). "The Design of Structures to Resist the Effects of Accidental Explosions."US
627 Department of the Army, Navy, and Air Force, Washington DC.
628 USGS (2013). "Seismic Hazard Analysis tools. U.S. Geological Survey." <
629 <http://earthquake.usgs.gov/hazards/designmaps/grdmotion.php>>.
630 Usmani, A. S. (2008). "Research priorities for maintaining structural fire resistance after seismic
631 damage". In Proceedings of the 14th world conference on earthquake engineering, Beijing.
632
633
634

635 **Fig. 1.** Conditional probabilities for cascading hazards

636 **Fig. 2.** Performance-Based earthquake Engineering for cascading hazards scenario

637 **Fig. 3.** Cyclic degradation for structural elements (FEMA P440A 2009)

638 **Fig. 4.** Lateral moment resisting frame configuration

639 **Fig. 5.** Internal bracing frame configuration

640 **Fig. 6.** Geometric configuration of the LPG tank

641 **Fig. 7.** LPG tank orientation with respect to the building façade

642 **Fig. 8.** Example of hazard sequence: earthquake-blast-fire

643 **Fig. 9.** (a) mean spectrum compatibility for 2% of exceedance probability in 100 years, (b) 5% of
644 exceedance probability in 100 years (reference range of period highlighted in grey)

645 **Fig. 10.** (a) probability to have leakage, (b) probability to have maximum fuel concentration, (c)
646 probability of ignition (according to IAOGP, 2010)

647 **Fig. 11.** Conditional probability of exceeding an IM for blast ($IM_B \geq im_B$) due to a given IM for
648 earthquake ($IM_1 = Sa(T_{tank}) \geq im_1$, $IM_2 = F_Q \geq im_2$)

649 **Fig. 12.** Fire compartments division for the building plan

650 **Fig. 13.** Building façade having a heat flux greater than 30 MJ/m² for each fuel quantity value

651 **Fig. 14.** Conditional probability of exceeding an IM for fire ($IM_F \geq im_F$) due to a given IM for blast
652 ($IM_B = F_Q \geq im_B$)

653 **Fig. 15.** (a) blast overpressure-time history for a face-on reflected wave; (b) idealized blast
654 overpressure time history (adopted by TM5-1300 1990)

655 **Fig. 16.** (a) Probability of exceeding a given damage state for earthquake hazard ($P(DS_E \geq ds_E)$) in X
656 direction; (b) Y direction

657 **Fig. 17.** (a) Probability of exceeding a slight, (b) moderate, (c) extensive, (d) complete damage state
658 for blast hazard ($P(DS_B \geq ds_B)$)

659 **Fig. 18.** (a) Probability of exceeding a irreversible damage on the beams, (b) irreversible damage on
660 the columns for fire hazard ($P(DS_F \geq ds_F)$)

665

Table 1. IM parameters values for earthquake

$P_{VR,E} [\%]$	50	20	10	5	2
$Sa(T_{ref}) [g]$	0.20	0.41	0.58	0.76	1.00

Note: $P_{VR,E}$ is the exceedance probability in 100 years for earthquake hazard.

666

Table 2. Selected exceedance probability for fuel quantity and associated values.

$P_{FQ} [\%]$	90	75	65	50	20	10	5	2	1
Fuel quantity [%]	55	62	67	70	77	80	86	92	100

Note: P_{FQ} is the fuel quantity exceedance probability.

Table 3. Number and localization of the compartments under fire for each fuel quantity value.

$P_{FQ} [\%]$	90	75	65	50	20	10	5	2	1
Fuel quantity [%]	55	62	67	70	77	80	86	92	100
Compartment area	C5	C5	C5	C4	C4	C4	C4	C4	C4
ID	C14	C14	C14	C5	C5	C5	C5	C5	C5
				C6	C6	C6	C6	C6	C6
				C13	C13	C13	C13	C13	C13
				C14	C14	C14	C14	C14	C14
				C15	C15	C15	C15	C15	C15
Compartment height	H1	H1	H1	H1	H1	H1	H1	H1	H1
ID					H2	H2	H2	H2	H2

Note: P_{FQ} is the fuel quantity exceedance probability.

667

Table 4. Selected exceedance probability for each generated heat flux.

$P_{qf} [\%]$	90	85	80	50	20	10	5	2
$q_f [MJ/m^2]$	135	160	180	230	281	322	360	400

Note: P_{qf} is the compartmental heat flux exceedance probability.

668

669

670

671

672

673

674

675 **Table 5.** Characteristic time-temperature curve parameters for each generated heat flux.

P_{qf} [%]	90	85	80	50	20	10	5	2
t_e [min]	23.50	25.00	26.19	33.46	40.83	46.85	52.2	58.2
T_{peak} [K°]	1111	1131	1145	1173	1188	1205	1218	1228
t_{peak} [min]	11.5	13.5	16	20.5	24.5	29.5	33.5	37

Note: P_{qf} is the compartmental heat flux exceedance probability.

676 **Table 6.** Uniform temperature in the cross section of the structural elements within the
677 compartments.

	Element	P_{qf} [%]							
		90	85	80	50	20	10	5	2
ΔT_{MAX} [K°]	W21x44	677	777	846	925	971	1,019	1057	1089
	W14x109	635	729	794	867	911	956	991	1021
	W12x136	560	643	700	765	804	843	875	901

Note: P_{qf} is the compartmental heat flux exceedance probability.

678 **Table 7.** Percentage of the stiffness reductions for each fuel quantity and earthquake HLs.

		P_{FQ} [%]								
		90	75	65	50	20	10	5	2	1
$P_{VR,E}$ [%]	50	62.28	71.96	74.63	76.89	87.5	92.77	96.53	97.20	98.98
	20	65.32	74.12	77.03	78.29	89.13	94.73	97.66	98.22	100.00
	10	68.76	79.74	80.83	85.18	93.19	98.52	99.83	99.75	100.00
	5	72.33	84.16	87.44	91.28	98.36	99.79	100.00	100.00	100.00
	2	79.52	89.59	93.89	97.85	100.00	100.00	100.00	100.00	100.00

Note: $P_{VR,E}$ is the exceedance probability in 100 years for earthquake hazard and P_{qf} is the compartmental heat flux exceedance probability.

679 **Table 8.** Blast Damage States and calculated stiffness reduction for blast analysis.

Blast Damage State (DS_B)	Slight	Moderate	Extensive	Complete
Drift [%]	1.00	1.80	2.80	4.80
Stiffness reduction [%]	30.00	61.00	75.00	85.00

680

681

682 **Table 9.** Numerical example for exceedance damage probability calculation due to earthquake, blast
683 and fire hazards, considering complete damage on the columns.

$P_{VR,E}$ [%]	$S_a(T)$ [g]	$S_a(T_{tank})$ [g]	$P(IM_B > im_B I_{M_E > im_E})$ [%]	$P(IM_F > im_F I_{M_B > im_B})$ [%]	$P(DS_E > d_{SE})$ [%]	$P(DS_B > d_{SB})$ [%]	$P(DS_F > d_{SF})$ [%]	$P(DS > ds)$ [%]
2	1,00	0.95	3.80	80.00	100.00	100.00	82.00	100.00
5	0.75	0.85	1.60	80.00	80.00	98.00	82.00	82.62
10	0.55	0.75	1.00	80.00	50.00	95.00	82.00	51.61
20	0.4	0.65	0.80	80.00	22.00	86.00	82.00	23.21
50	0.2	0.4	0.45	80.00	1.50	55.00	82.00	2.04

Note: $P_{VR,E}$ is the exceedance probability in 100 years for earthquake hazard.

HAZARD

Hazard 1



Hazard 2



Hazard 3



PROBABILITY OF EXCEEDING A GIVEN INTENSITY MEASURE

$$P(IM_1 \geq im_1)$$

$$P(IM_2 \geq im_2) = P(IM_2 \geq im_2 | IM_1 \geq im_1) \cdot P(IM_1 \geq im_1)$$

$$P(IM_3 \geq im_3) = P(IM_3 \geq im_3 | IM_2 \geq im_2) \cdot P(IM_2 \geq im_2 | IM_1 \geq im_1) \cdot P(IM_1 \geq im_1)$$

Hazard analysis

$$p(IM)$$



hazards interaction

$$p(IM_i | IM_{i-1})$$

Structural analysis

$$p(EDP | IM, SP)$$



$$p(EDP)$$

Damage analysis

$$p(DM | EDP)$$



$$p(DM)$$

Loss analysis

$$p(DV | DM)$$

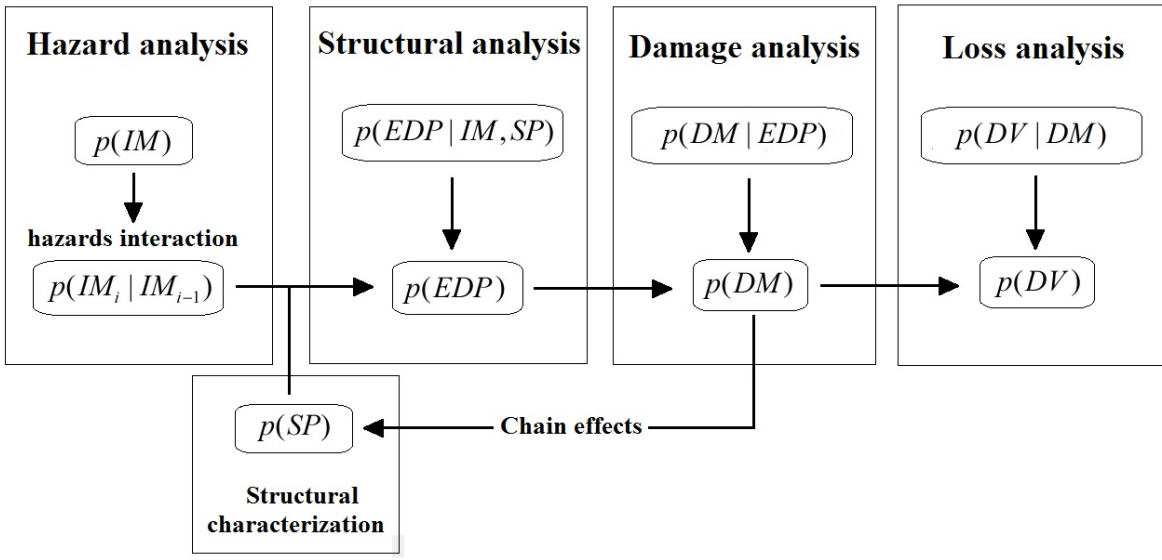


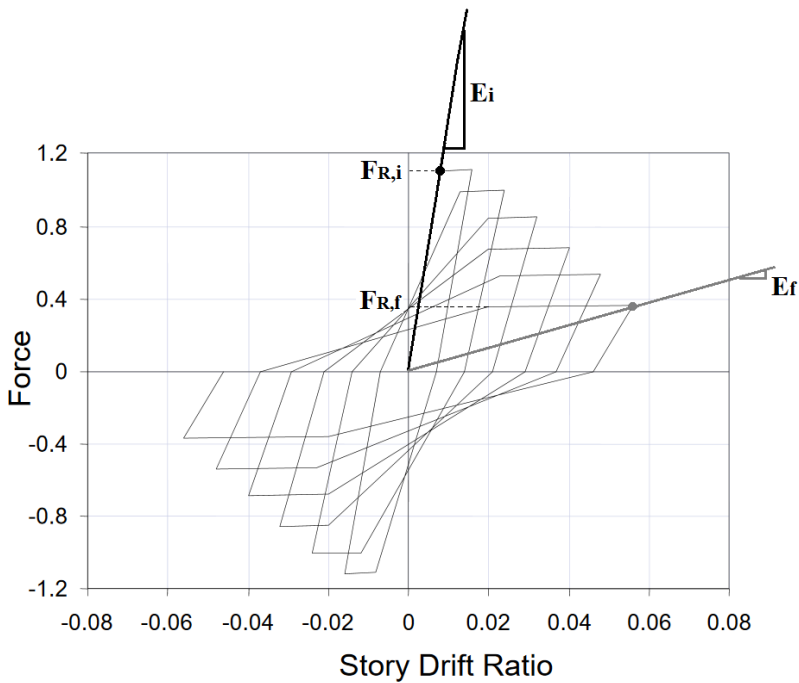
$$p(DV)$$

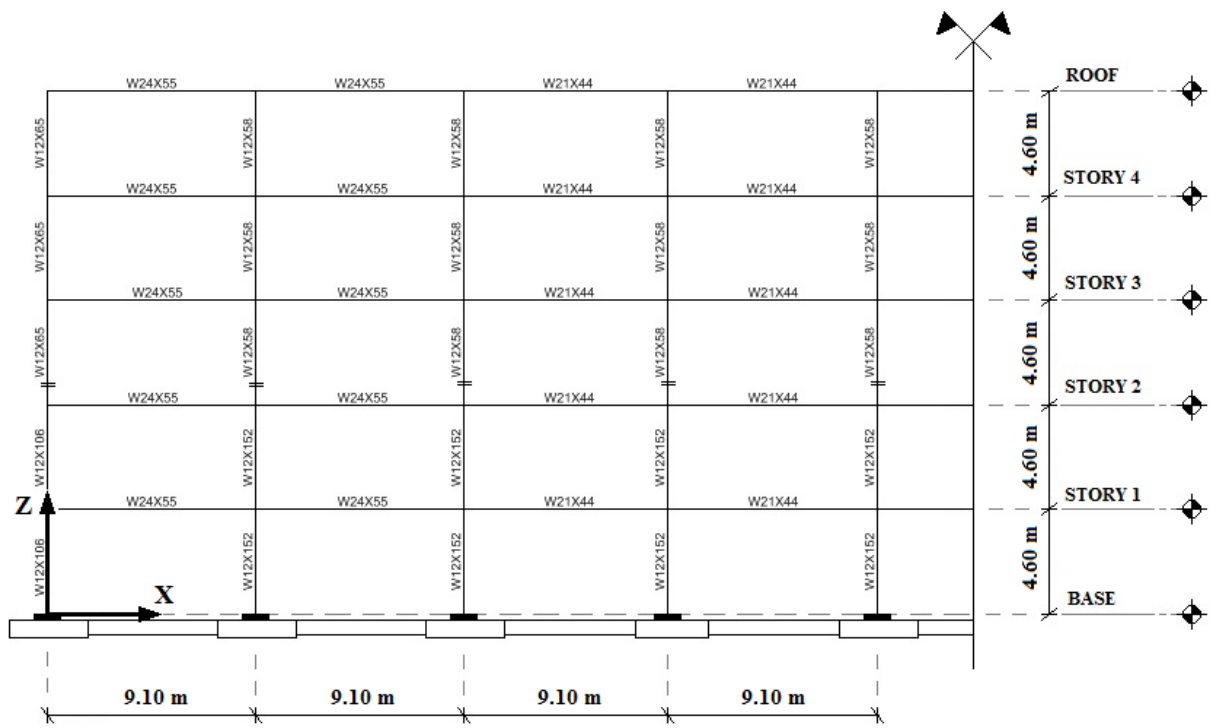
$$p(SP)$$

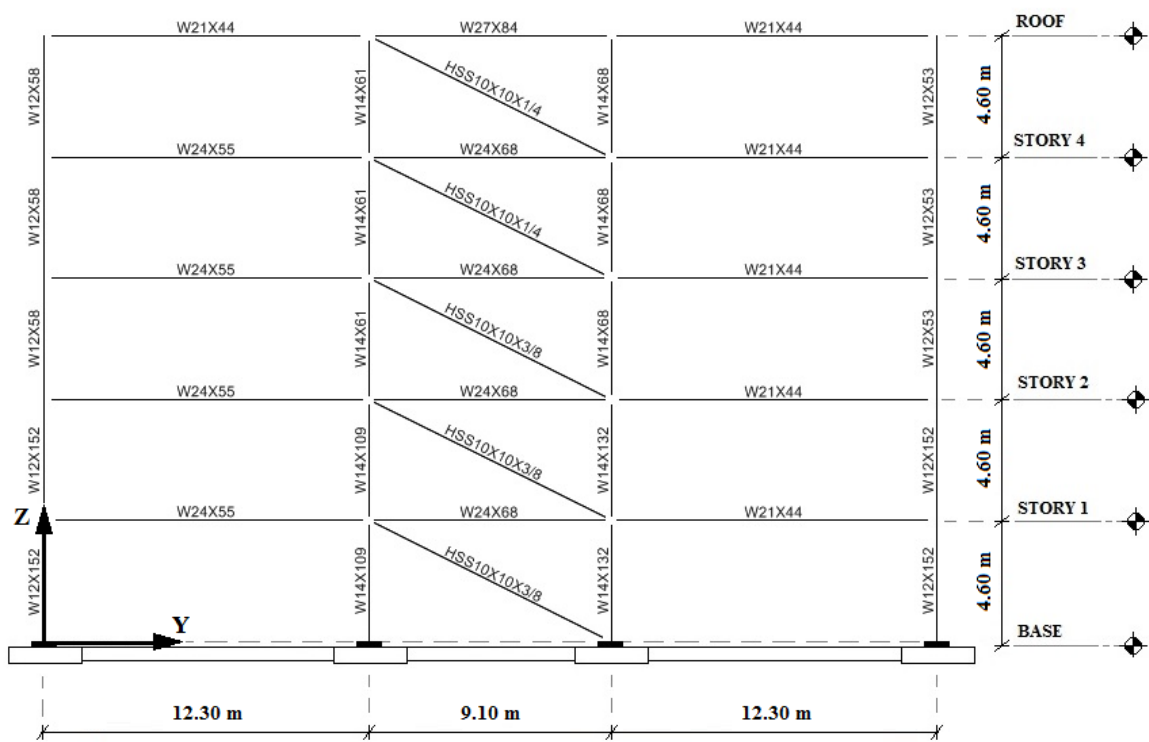
**Structural
characterization**

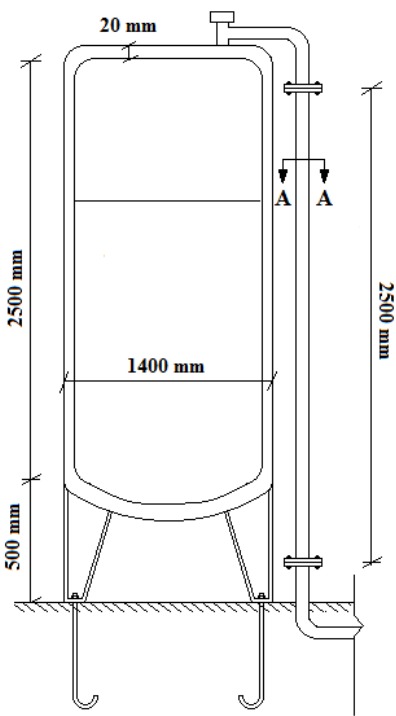
Chain effects



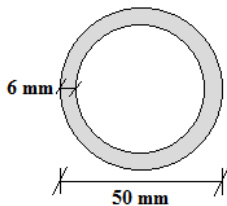


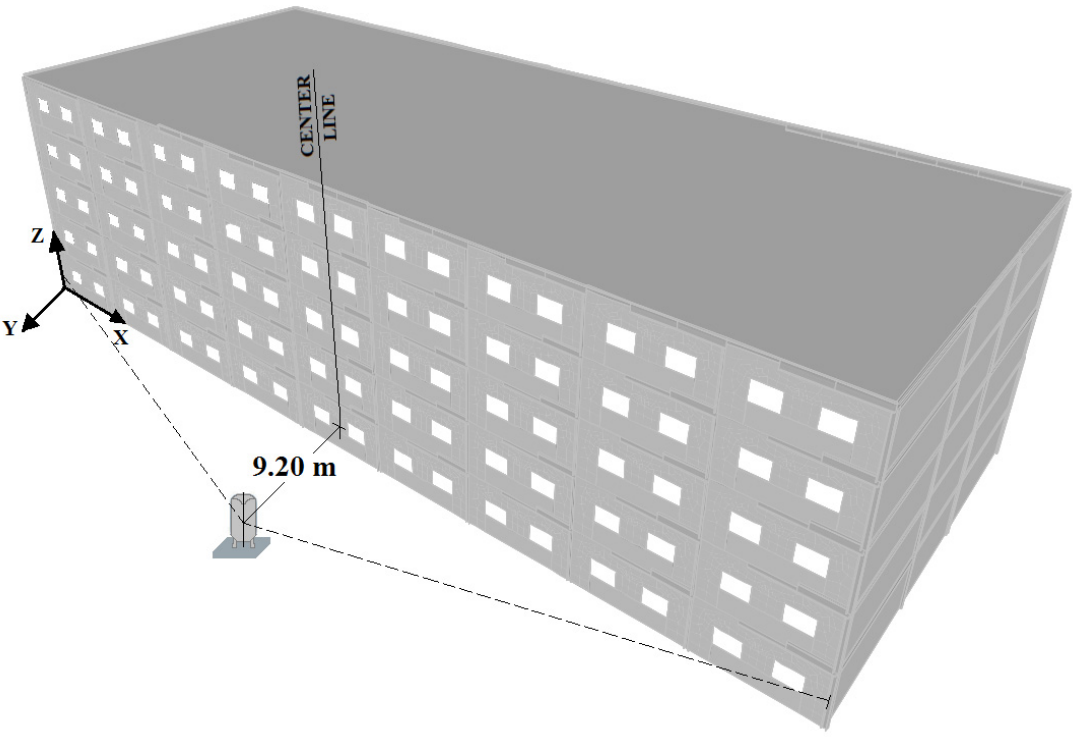


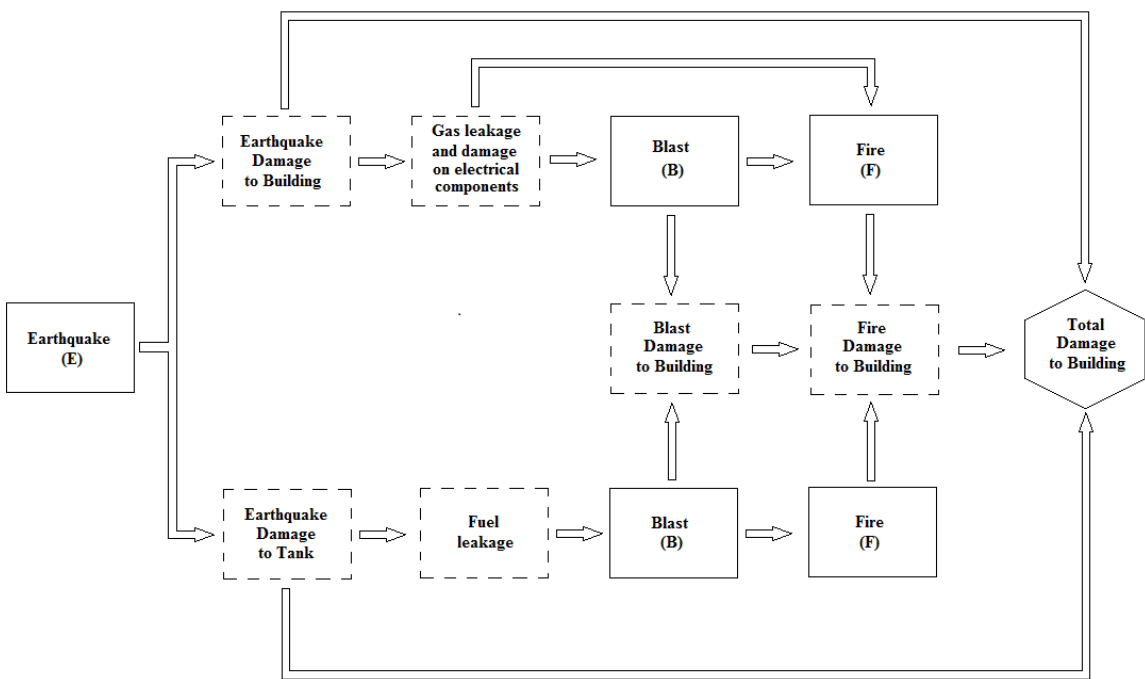


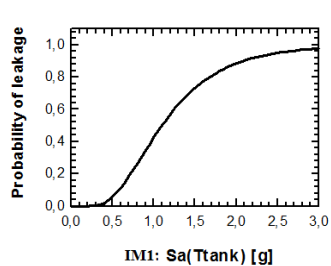


Section A-A

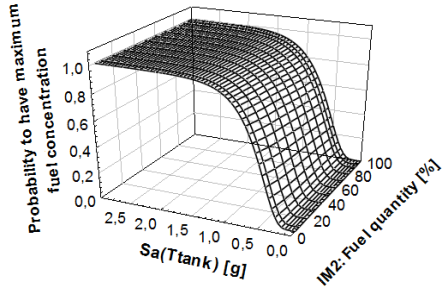




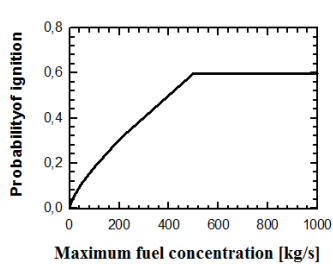




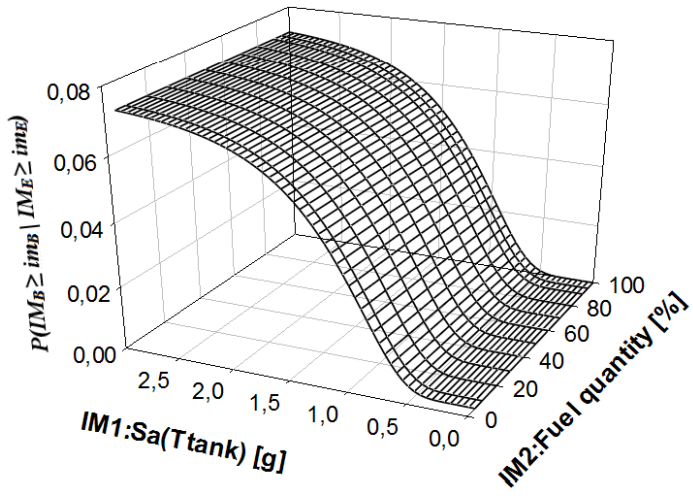
(a)

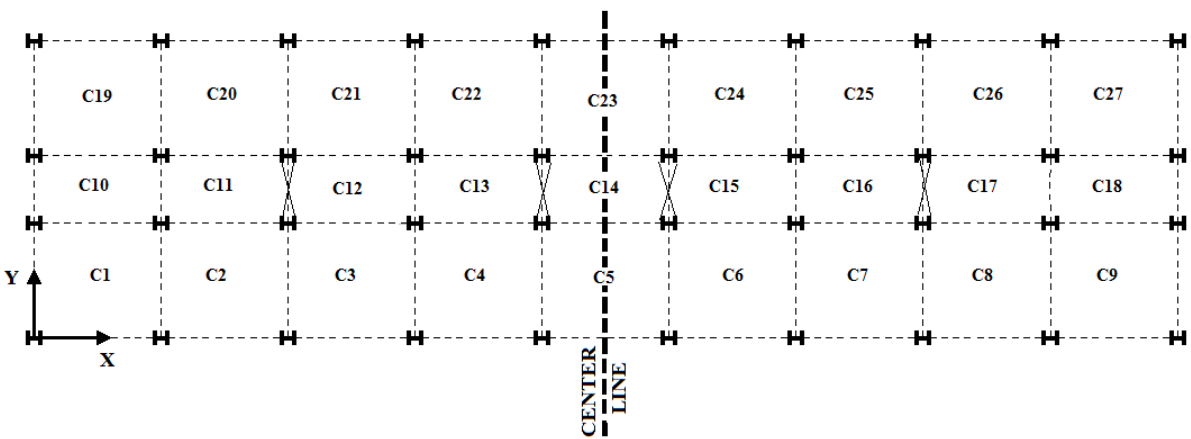


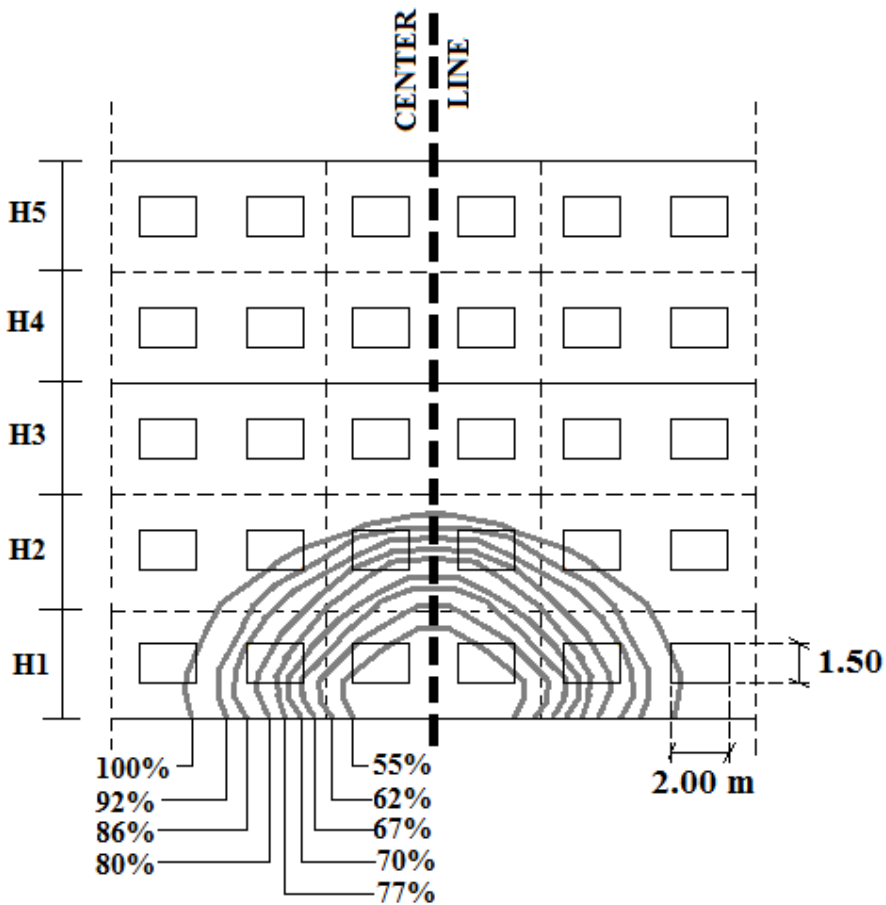
(b)

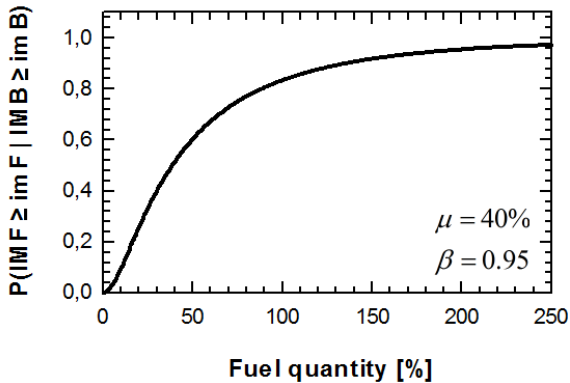


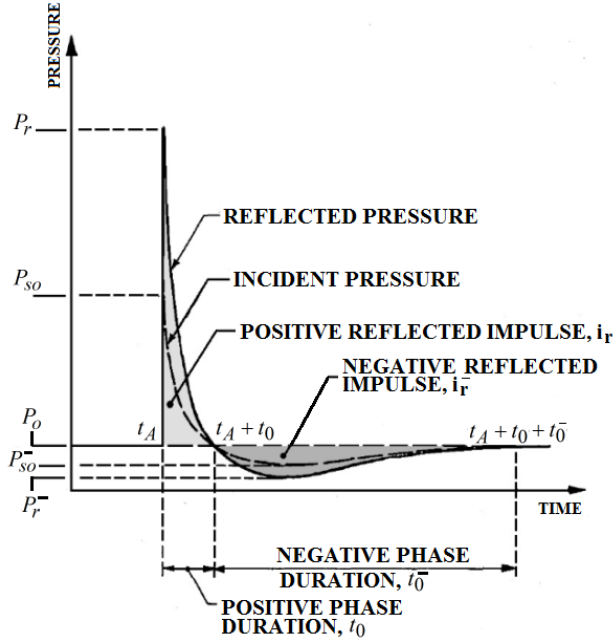
(c)



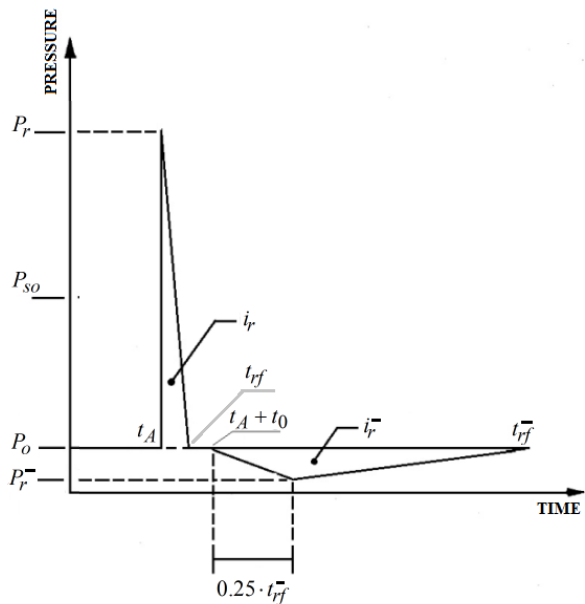




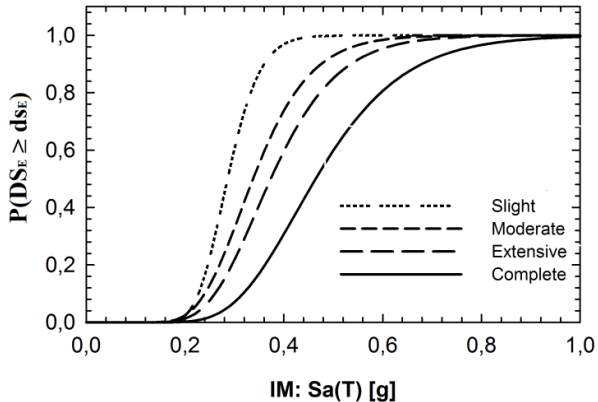




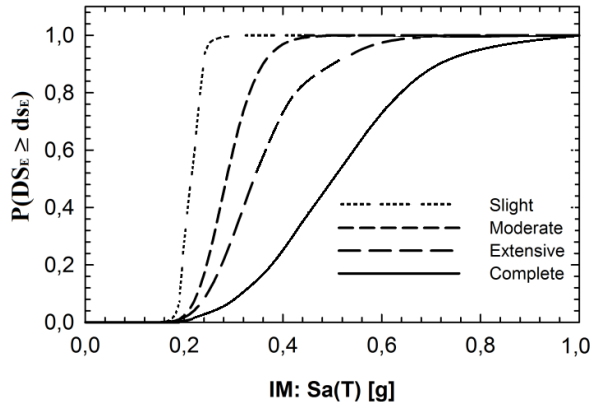
(a)



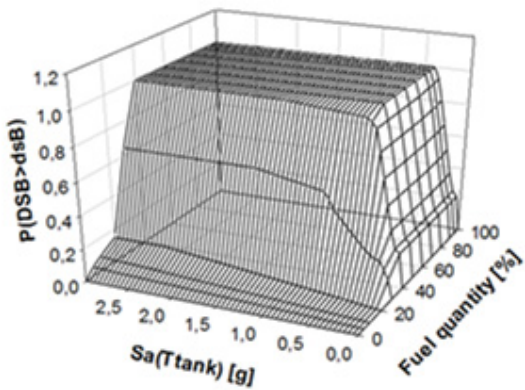
(b)



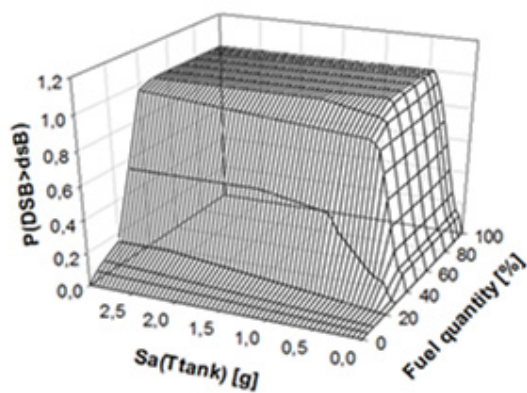
(a)



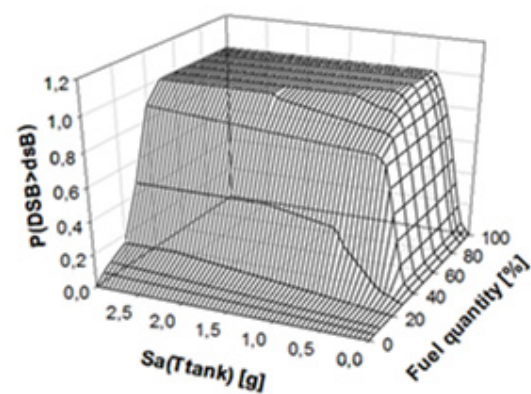
(b)



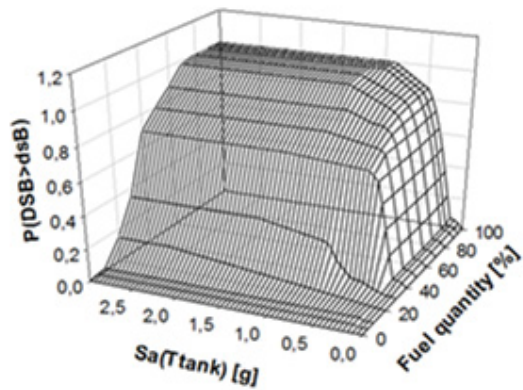
(a)



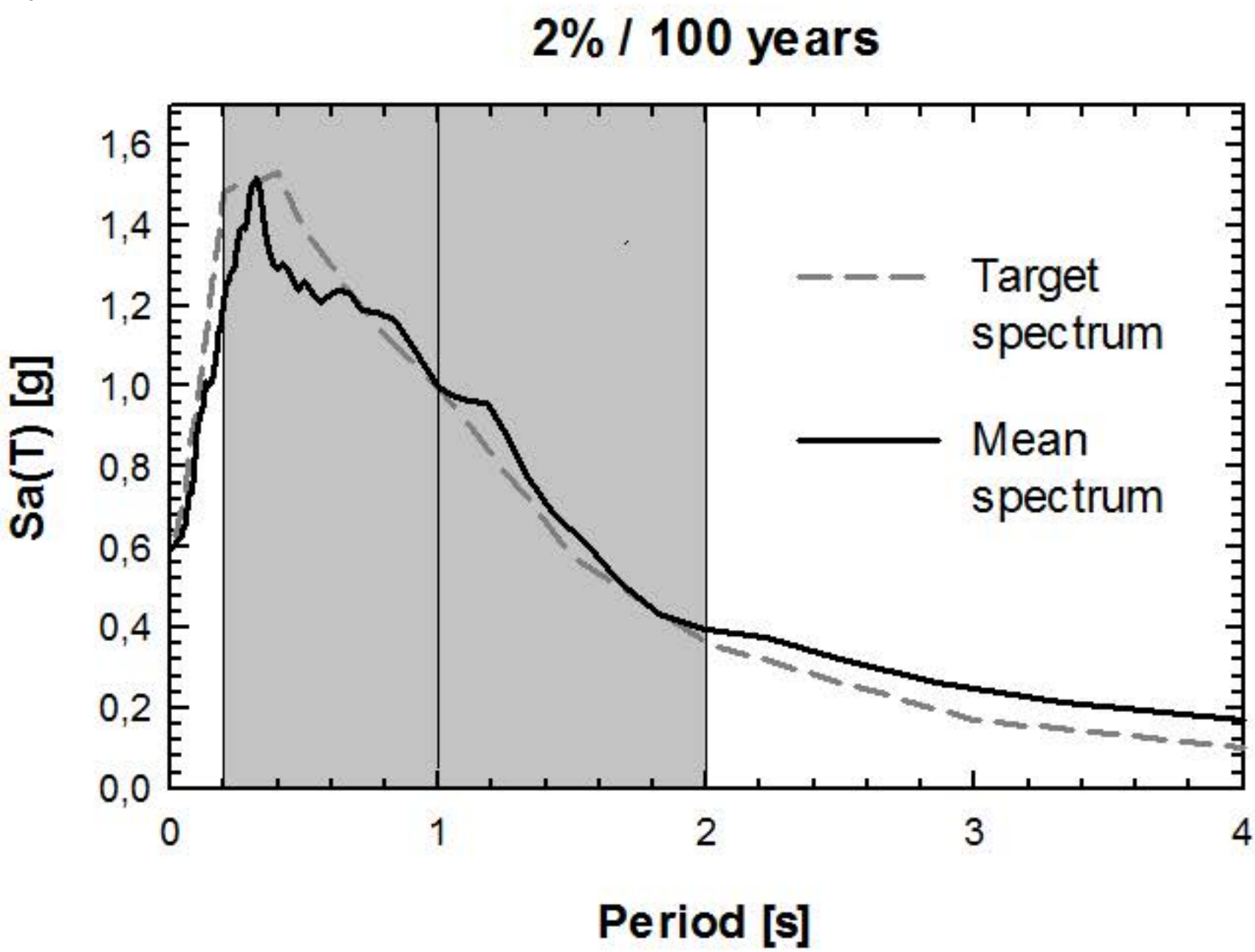
(b)



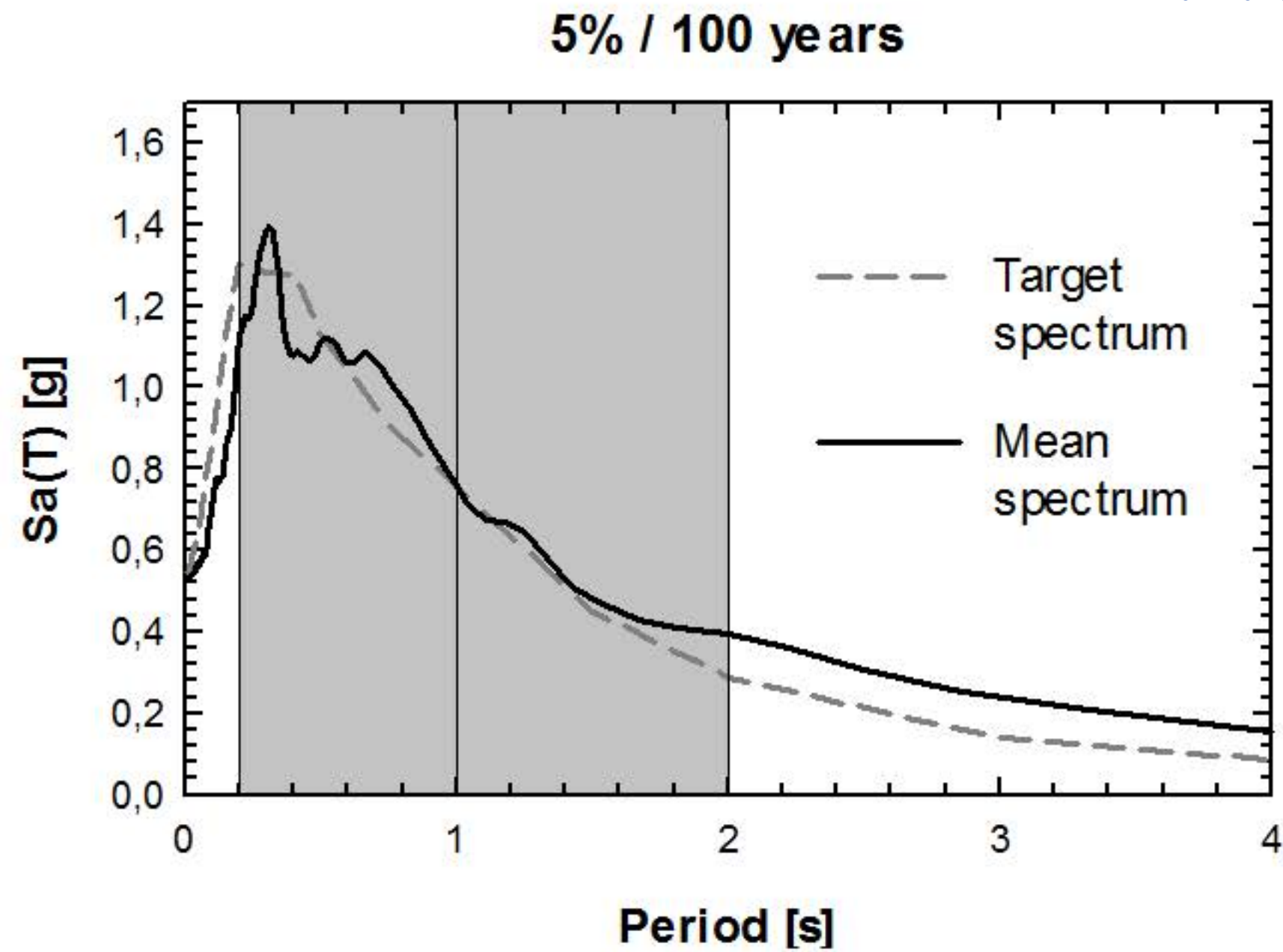
(c)



(d)



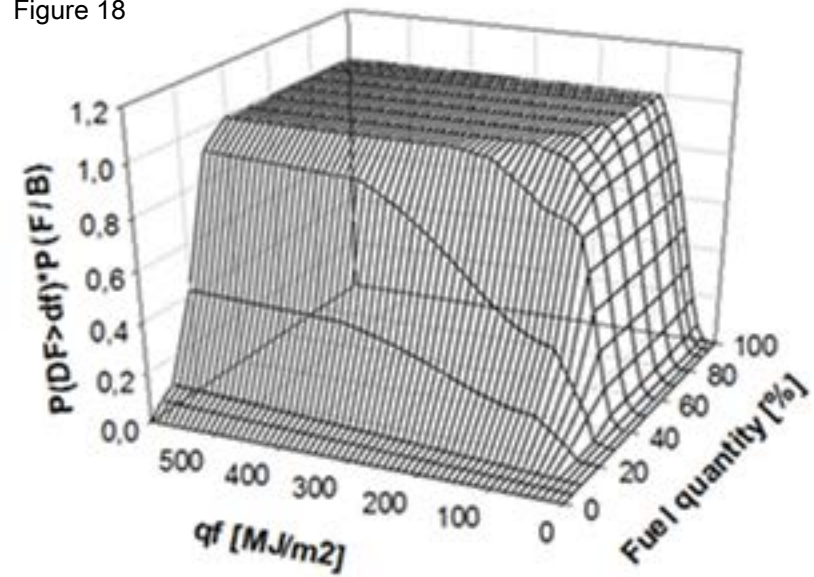
(a)



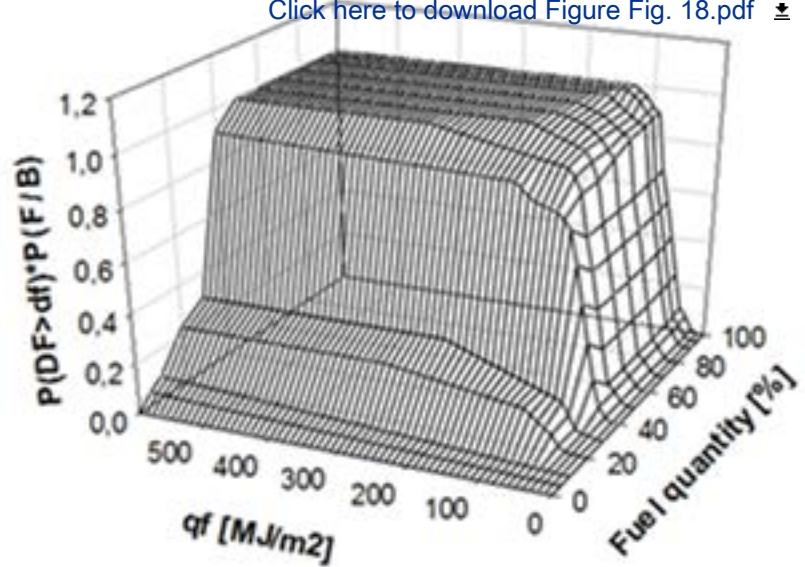
(b)

Figure 18

[Click here to download Figure Fig. 18.pdf](#)



(a)



(b)